JOURNAL OF MATERIALS SCIENCE **36** (2001) 3335–3341

Microstructural features associated with spray atomization and deposition of Al-Mn-Cr-Si alloy

A. K. SRIVASTAVA
Electron Microscope Section, Division of Materials Characterization, National Physical Laboratory, New Delhi 110 012, India

S. N. OJHA
Centre for Advanced Study, Department of Metallurgical Engineering, Banaras Hindu University, Varanasi 221 005, India

S. RANGANATHAN
Centre for Advanced Study, Department of Metallurgy, Indian Institute of Science, Bangalore 560 012, India

An inert gas atomization process was employed in production of rapidly solidified powders as well as disc-shape preform by spray deposition of an $Al_{75}Mn_{10}Cr_5Si_{10}$ alloy. Microstructural features of atomized powders and spray deposited preforms were evaluated by scanning and transmission electron microscopy and X-ray diffractometry techniques. Solidification structure of powders revealed cellular and dendritic morphology, depending on their size. The interdendritic regions consisted of second phase particles. In contrast the spray formed alloy exhibited microstructural homogeneity with distribution of ultra-fine second phase particles of intermetallic compound. The structure of second phase intermetallics was identified as a cubic α-Al(Mn,Cr)Si, in both the atomized powders and the spray-deposits. The formation of cubic phase is discussed as rational approximant structure of an icosahedral quasicrystal.

1. Introduction

The process of spray forming refers to the energetic disintegration of molten metal by high velocity gas jets in micron-size droplets and the subsequent deposition of the mixture of solid, liquid and partially solidified droplets on a substrate [1–6]. The technique has fascinated to its capability of producing near net shape products in single step, with inherent rapid solidification effects [7–13]. In recent years, several Al-based alloys, required for high strength and high temperature applications, have been synthesized using this method.

Al-Mn-Cr-Si system has been considered for elevated temperature service for several reasons [14–18]. In Al-Mn-Cr, both Mn and Cr have low solid solubilities under equilibrium conditions and low diffusivities at high temperatures [19–21]. The solid solubilities of Mn and Cr could be extended from 0.76 to 9 at% for Mn and from 0.44 to >6 at% for Cr, when cooling rates in the range of 10^6 to 10^7 K/s were used [22]. Rapidly solidified Al-5Mn-2.5Cr alloy powders [19] smaller than the mass median size of 9 μm revealed a complete absence of the second phase while increasing amounts of icosahedral I-phase, Y-AlMnCr and θ-Al_7Cr were present in larger powder particles. Increasing the Cr in Al-Mn-Cr alloy [23, 24] resulted in extensive precipitation of θ-$Al_{13}Cr_2$ and a decrease of supersaturation during rapid solidification. Icosahedral phase and irrationally twinned cubic crystals α-Al(Mn, Cr)Si phase were identified as an important microstructural constituent of a rapidly solidified Al-Mn-Cr-Si alloy [25–27]. A new metastable orthorhombic phase with a B-centered unit cell, which transformed slowly to the G-phase, $Al_{12}(Mn, Cr)$, upon annealing, was analyzed [28, 29]. The morphology of the icosahedral phase and the orientation relationship with α-Al matrix has been studied [30]. The structural similarity and orientation relationship between α-AlMnSi(Cr) and metastable orthorhombic phase in this alloy has also been reported [31, 32]. However, these alloys are processed by rapid solidification and powder metallurgy methods.

The inert gas atomization of Al-Mn alloys, led to particulates or powders, subsequently consolidated by rolling or extrusion. The potential of the spray forming process has not been fully exploited. In the present investigation, spray-forming process was employed to synthesize the $Al_{75}Mn_{10}Cr_5Si_{10}$ alloy. The process eliminated several intermediate steps of powder metallurgy methods of materials consolidation. The solidification structure associated with atomized powders and its role in the microstructural evolution in spray deposited preforms was studied. Efforts were made to understand the structure and microstructure of second phase dispersoids. Formation of cubic α-Al(Mn,Cr)Si

in atomized powders and preform produced by spray deposition is discussed.

2. Experimental procedure

Alloy corresponding to composition $Al_{75}Mn_{10}Cr_5Si_{10}$ was prepared by induction melting 4N purity aluminium with high purity Mn, Cr and Si in graphite bonded fireclay crucible. Continuous supply of argon gas was maintained in the crucible during melting the alloy to protect the melt from oxidation.

The rapidly solidified powders were produced by inert gas atomization process. The details of the atomizer have been described elsewhere [5, 33]. In brief, the process makes use of an annular convergent-divergent nozzle to generate high velocity gas jets. The nozzle of 5-mm diameter was used for this purpose. The liquid metal in this process is brought down through a flow tube co-axial with the nozzle. The gas jet initially interacts with the melt stream at the tip of the flow tube to promote atomization. Although the process can be used in both upward and downward atomization modes, the latter has been employed in the present experiment. Nitrogen gas was initially run through the nozzle to purge the atomization chamber. The gas at 1.5 MPa gas pressure subsequently atomized the melt. The weight of powders and duration of atomization provided a melt flow rate of 1.2 kg min^{-1}. The gas flow rate of 3.0 kg min^{-1} was consistently maintained in all the experiments. The powders were sieved into various size fractions for microstructural analysis.

To produce spray deposited preforms of the alloy, a copper substrate was introduced at 25 cm, below the atomization nozzle. The melt was atomized with the same processing conditions and the resulting spray of droplets was deposited on the copper substrate to obtain a preform of 20 cm diameter and 8 mm thickness.

Several samples were machined from different regions of the preform for microstructural examination. In addition, powders of three different size fractions were mounted in bakelite. The samples were polished following standard metallographic procedures. A dilute Keller's reagent (95% H_2O–2.5% HNO_3–1.5% HCl–1% HF) solution was used to etch polished cross-sections of the samples. The microstructure of the samples was examined in a JEOL JSM 840A scanning electron microscope (SEM) operated at 20 kV.

The structure of second phase intermetallics along with the α-Al matrix in atomized powders as well as in spray-deposited alloys were identified by X-ray diffractometry (XRD) technique. The Enrauf–Nonius X-ray generator, operated at 40 kV and 200 mA and Huber diffractometer were used for this purpose.

To understand the size, nature and distribution of aluminium-rich intermetallic dispersoids in spray deposited alloy, a further study at high magnification was proceeded using transmission electron miscroscopy (TEM). TEM samples of spray deposited foils were prepared by electropolishing and ion beam techniques. Electropolishing was performed using chemical solution of 80% methanol and 20% nitric acid at $-30°C$. Ion-beam milling was carried out using 6 keV Ar^+ and at beam incident angle of $\sim 20°$ on the specimen. The specimens were examined in a JEOL JEM 2000 FX-II electron microscope, operated at 200 kV

3. Results and discussion

3.1. Microstructural characteristics of atomized powders

The results of the sieve analysis indicated a wide size range of particle aggregate with 80% powders to be below 150 μm size. A cumulative wt.% polygon of atomized powders with their size distribution provided median particle diameter (d_m) of 70 μm, whereas d_{84} (84 cumulative wt.%) and d_{16} (16 cumulative wt.%) were 124 μm and 32 μm, respectively (Fig. 1a). The above three characteristic diameters represent the particle size distribution. In addition, fine powders (below 150 μm) exhibited a bimodal size distribution with the maximum yield of powders occurring between $-75+53$ and $-120+90$ μm size ranges (Fig. 1b). It is considered that the bimodality is beneficial during powder compaction.

It was seen that the most of the fine powders have a spherical shape in contrast to the irregular shape of the coarse particles. Some of the particles also showed

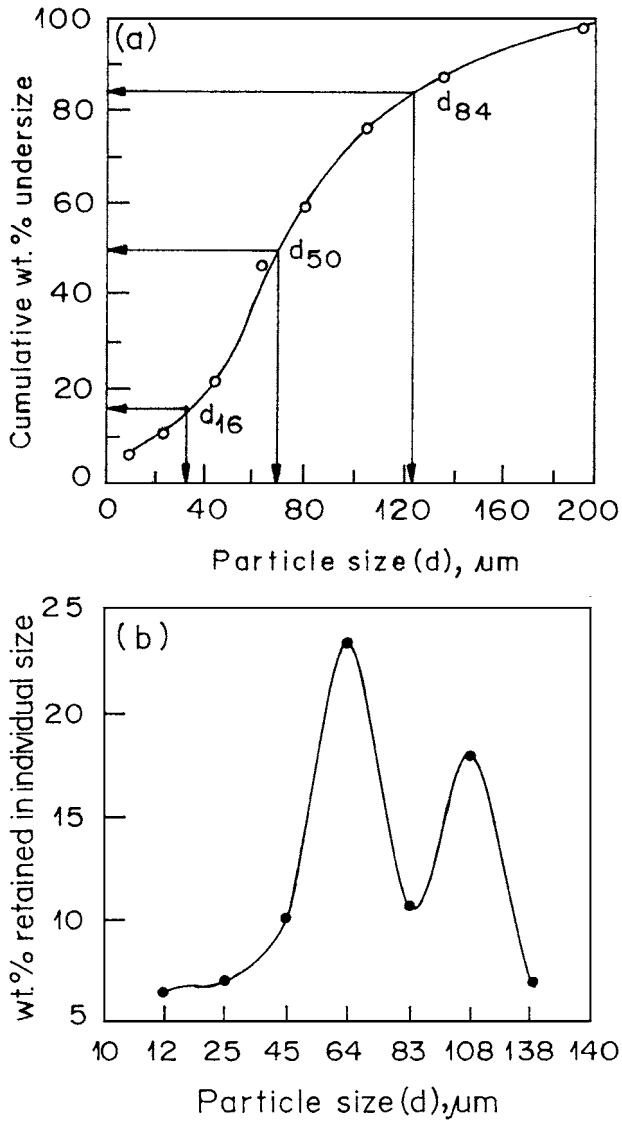

Figure 1 (a) Cumulative wt.% polygon of atomized powder particles and (b) wt.% retained in individual size distribution.

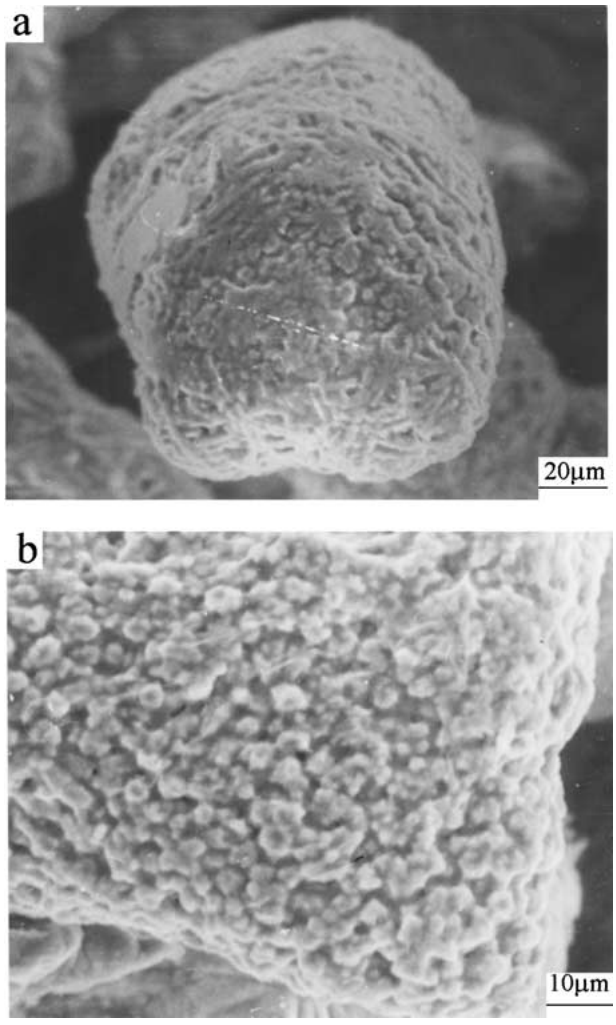

Figure 2 SEM micrographs of atomized powder particles showing dendrites and cored feature (a) and (b).

dumbbell shape. The surface microstructure exhibited cellular-dendritic growth morphology. In addition, the striking feature of coarse particles was the presence of cored dendrite microstructure (Fig. 2). The cored dendritic growth feature of powders has been found favourable for the formation of equiaxed grain during subsequent stages of spray deposition.

The microcellular region in atomized powders depends on the velocity of solid–liquid interface. Initially, this velocity is large in the undercooled droplet and generates cellular structure near the nucleation site [1, 5]. As the growth proceeds, the recalescence of the melt occurs with a consequent increase in the interface temperature. This situation destabilizes the interface and favours cellular and dendritic growth during later stages of solidification of the droplet. Since the recalescence of the melt is so rapid that it is difficult to suppress this effect even with high heat exchange rate at the droplet–gas interface in atomization and also as the interface temperature exceeds the temperature for supersaturation, the solute is rejected ahead of the interface, the stability of the interface further gets disrupted. Therefore decreasing the size of the droplet can enhance the microcellular region.

Atomization of melt is the first step in spray forming. Partially solidified metal droplets are dispersed on a substrate to produce fine-grained microstructurally homogeneous material. The size and spatial distribution of droplets are of interest as the deposit shape resembles the spatial distribution of droplets mass arriving on the deposition surface and solidification structure of droplets govern the microstructure of deposit.

3.2. Microstructural features induced by spray deposition

Specimens prepared from the center of the deposit showed considerable refinement in the microstructure with a uniform distribution of second phase particles. Additionally uniformity in the microsructure was discerned throughout this region of the deposit. Samples from the peripheral sections of the spray deposit exhibited some variation in the scale of the microstructure. Fig. 3a shows a homogeneous fine scale distribution of ultrafine second phase in particles in a fine-grained matrix. The shape of the second phase has facetted growth morphology. The microstructural examination also showed fine dendrites at the top region of the preform generated towards the end of deposition process (Fig. 3b). The secondary dendrite arms were not sharp and rather skewed and tending towards the formation of equiaxed grains (Fig. 3b). This feature is attributed to the deformation induced in the semi-solid droplet during impact on the growing deposit. Prior particle boundaries were also observed in the top region of the deposit, surrounded with a liquid flow line created on the deposition surface (Fig. 3c).

The section of the deposit also revealed submicroscopic porosities distributed along grain boundaries. Pores of 1 to 5 μm sizes were observed in the microstructure. Conventional density measurements carried out on specimens prepared from different regions of the deposit showed that the density of the material was approximately 97% of theoretical density. The maximum porosity was observed in the samples prepared from the peripheral sections of the preform.

Heat transfer conditions existing during atomization and after the liquid alloy droplets impacted on the substrate or the deposition surface influences the microstructure of the spray formed deposit. As a consequence the size, nature and size distribution of intermetallics, which are one of the most important characteristics of rapidly solidified dispersion–strengthened alloy, depened on the processing conditions maintained during deposition. Microstructural variation observed at the top surface of the preform has revealed some interesting features (Figs 3b and c). The grain size observed in this region varied than the rest of the section of preform. Fine dendrites were also seen in the top region of the prefrom. The decreasing metal flow rate, with a consequent decrease in spray density and resultant size of droplets, towards the end of the experiment, the splats solidify completely before the arrival of the next droplet. Because of the small droplet size and accordingly, the high velocity of droplets, their cooling rates are relatively achieved high. Additionally, the violent splatting action against a rigid surface, the thinness of the splats and the undercooling of the droplets all

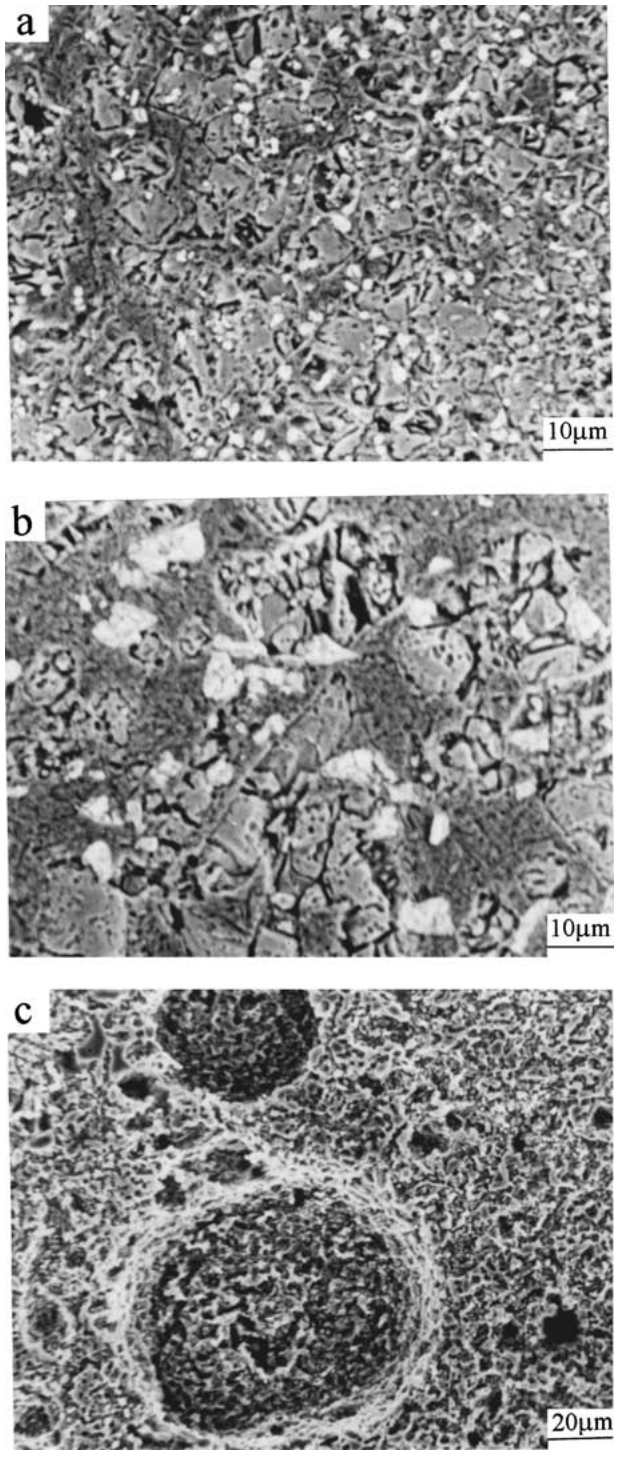

Figure 3 SEM micrographs showing (a) fine grains throughout central region of the deposit, variation in microstructures at the top regions of the deposit; (b) fine dendrites and (c) prior particle boundaries.

contribute to the formation of a fine-grained microstructure. Furthermore, as the average droplet size decreases during atomization, the proportion of solidified droplets arriving at the deposition surface increases and some of them retain their spherical morphology on impact. Because in this compaction process there are individually solidified splats, there exist irregular interstices that cannot be filled with the liquid and, accordingly, porosity levels will increase relative to the lower part of the compact. A fine dendritic microstructure seen in this region is attributed to a relatively slow cooling rate of large size droplets during atomization stage and the microstructure of partially solidified droplets are still left out in the deposit. From the microstructural feature it can be deduced that the arms of these dendrites are skewed and are acting as fractured dendrites.

Observation of cored dendrite structure of the primary phase in atomized powders provides an insight into formation of equiaxed grain morphology during deposition. Several mechanisms have been proposed to explain the microstructural evolution during spray deposition [2, 3, 5, 7, 8]. The heat extraction rate at the substrate is lower than the heat input at the upper surface and this leads to the formation of a molten layer on top of the deposit [1, 3]. During deposition, dendrite arm fragmentation, nucleation/grain multiplication and constrained growth are presumably simultaneous mechanisms contribute to the evolution of fine grain microstructure [1]. In addition, growth and coalescence during annealing of material at high temperature for a finite period of time [2] and also same second phase formation, precipitation etc, may occur in the deposited material during annealing. Under steady state deposition conditions the deposit has been reported to contain between 60–80% solid and due to impact of high velocity droplets on the growing deposit, shear action also induces recrystallization in the solid fraction of the droplets [7, 8].

3.3. Structure and morphology of second phase intermetallic

The identification of second phase dispersoids in atomized powders as well as in spray deposited alloys was carried out by X-ray diffraction method. Fig. 4 shows

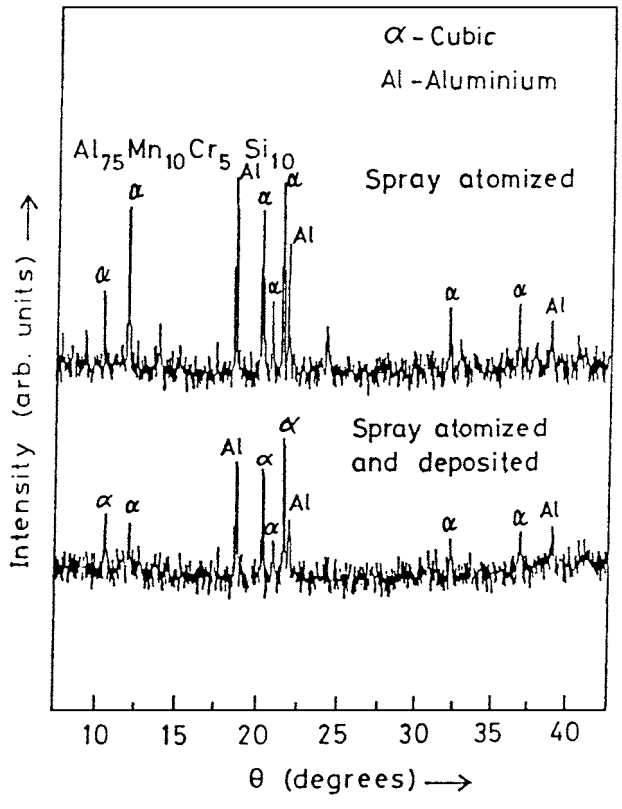

Figure 4 XRD patterns showing the presence of a cubic α-Al(Mn, Cr)Si phase along with α-Al in spray atomized and spray atomized & deposited conditions.

XRD recorded from atomized powders as well as that of the spray deposited alloy. It is worthwhile to note that both the atomized powders and spray deposited alloy show the existence of cubic α-Al(Mn, Cr)Si phase alongwith α-Al matrix. The lattice parameter calculated for the cubic unit cell of α-Al(Mn, Cr)Si corresponded to 12.69 Å.

TEM study on spray deposited alloy indicated the distribution of ultra-fine second phase particles in the matrix phase (Fig. 5a). These particles, as also evidenced by XRD were identified as cubic α-Al(Mn, Cr)Si phase uniformly distributed in the α-Al matrix. The distribution of second phase particles under spray deposited condition was homogeneous with an average size of about 0.5–1 μm. It was interesting to note that the cubic phase observed in this alloy is a rational approximant structure of the icosahedral quasicrystal. It was noticed by seeing the intensity, modulation in diffraction spots recorded from α-Al(Mn, Cr)Si phase along [001], [$\bar{1}$11] and [023] zone axes of cubic structure (Fig. 5b–d). The important diffraction spots have also been indexed in these patterns. The rational approximant aspect of α-Al(Mn, Cr)Si will be discussed in the context of nature of second phase particles.

The addition of ternary and quaternary elements to binary alloys leads to the formation of intermetallics with a more symmetrical lattice [12]. A ternary phase, known to exist in Al-Mn-Cr alloys under equilibrium conditions, has been reported to be a G-Al_{12}(Mn, Cr) [29]. It is important to note that the G phase is metastable in binary Al-Mn. Equilibrium ternary intermetallics reported in Al-Mn-Si are: α-AlMnSi and β-AlMnSi in Al-rich alloys [16, 17]. It has also been reported that the cubic α-Al(Mn, Cr)Si phase is structurally and chemically related to the icosahedral quasicrystal [15, 26]. The lattice parameter of cubic cell of α-Al(Mn, Cr)Si, calculated in present work is in agreement with that reported lattice parameters of α-Al(Mn, Cr)Si [26] and α-AlMnSi ($a = 12.68$ Å) [16, 17].

Studies carried out on Al-Mn alloy system have led to the conclusion that the cubic phase α-Al(Mn, Cr)Si

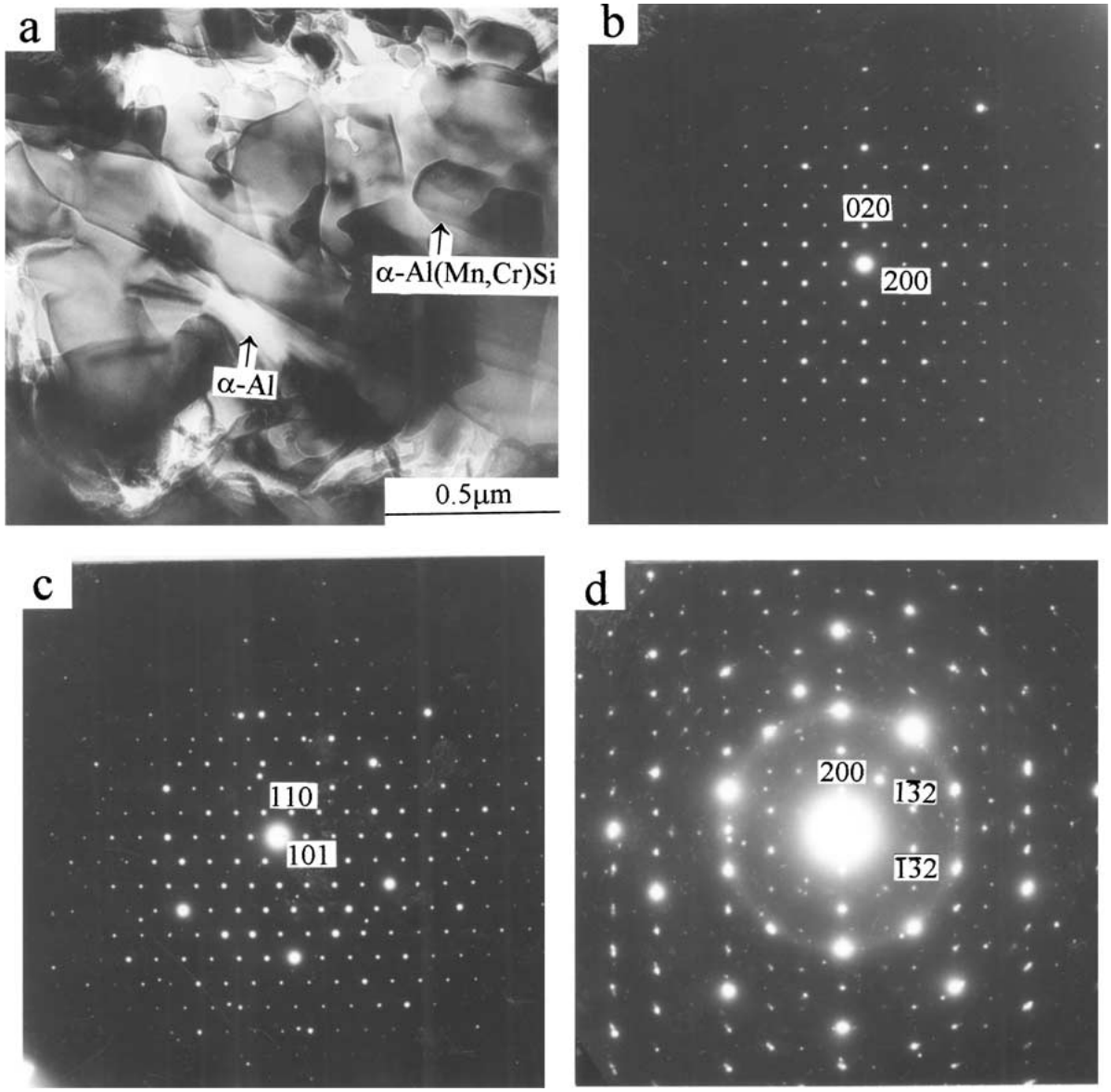

Figure 5 TEM (a) bright field micrograph showing dispersion of α-Al(Mn, Cr)Si phase and corresponding electron diffraction patterns along (b) [001], (c) [$\bar{1}$11] and (d) [023] zone axes of cubic structure.

TABLE I Commonly occurring phases, their structure and morphology in Al-Mn-Cr-Si alloys

Phase	Morphology	Crystal system	References
i-Al(Mn, Cr)Si	worm-like, equi-axial	icosahedral	Singh *et al*. [25], Srivastava and Ranganathan [26], Guo *et al*. [30]
α-Al(Mn, Cr)Si	spherical	cubic	Present work, Singh *et al*. [25] Srivastava and Ranganathan [26] Guo *et al*. [31]
G-Al_{12}(Mn, Cr)	—	cubic	Liu *et al*. [19], Waterloo *et al*. [28]
−Al(Mn, Cr)Si	needle/plate	orthorhombic	Waterloo *et al*. [28], Anderson *et al*. [32]

is a rational approximant to the icosahedral quasicrystal [15, 26]. The cube vectors $\langle 001 \rangle$ and $\langle 111 \rangle$ belong to 2-fold and 3-fold vectors of an icosahedral quasicrystal, whereas cube vectors $\langle 023 \rangle$ are related to vectors $\langle 01\tau \rangle$, where τ is the golden mean ($\tau = 1.618034\ldots$). The intense spots in the diffraction patterns of α-Al(Mn, Cr)Si as shown in Fig. 5b–d, agree well with the positions of spots in 2-fold, 3-fold and 5-fold patterns of the icosahedral quasicrystal [25]. It has been stated that the best icosahedral (AlMnSi) composition is $Al_{74}Mn_{20}Si_6$ and the composition of α-(AlMnSi) is very near to this value, $Al_{72.5}Mn_{17.4}Si_{10.1}$ [15]. Several interesting non-equilibrium microstructures have been reported, under rapid solidification. The evolution of important phases, their morphology and crystal structures have been summarized in Table I. During processing, a small fluctuation in solidification time and composition leads the transition from icosahedral quasicrystalline phase to a crystalline phase or vice versa. A detailed microstructural characterization of the alloy, processed by rapid solidification melt spinning technique has been earlier reported [25, 26]. In melt spun foils of Al-Mn-Cr-Si alloy, fine size α-Al(Mn, Cr)Si cubic crystallites of about 0.3 μm at the periphery of the icosahedral grains ($\sim$3 μm) exhibited a multiple twinning around an irrational axis. Selected area diffraction patterns showed that the crystalline aggregate symmetry is linked with the icosahedral point group symmetry. In another observation, the rapidly solidified powder particles less than 25 μm size of Al-Mn-Cr alloy showed that virtually all of the precipitates in the lower Cr-content alloy are the icosahedral phase while on increasing the Cr–content θ-(Al, Cr) phase predominated with only occasional icosahedral precipitates [23]. The second phase particles observed in the present work, is extremely fine with a characteristic spherical morphology [25, 26, 31]. However, the twining evidences of intermetallics leading to icosahedral symmetry are not seen in both atomized powders as well as in spray deposited alloy. On the other hand, in spray deposited condition, the particles are observed to randomly distribute within the fine grain α-Al matrix.

4. Conclusions

1. The N_2 gas atomized powders of Al-Mn-Cr-Si alloy exhibits a characteristic bimodal size distribution. The polygon of cumulative wt.% distribution of the sieve analysis data yields a median particle diameter of 70 μm with standard deviation of size distribution as 1.8. Small size powder particles reveal spherical shape against the irregular shape of coarse particles.

2. The atomized powders reveal a cellular-dendritic growth morphology of the primary phase with a dispersion of cubic crystalline silicide intermetallic phase in the intercellular or interdendritic regions. The microstructural features of powders evidenced for heterogeneous nucleation occurring from the surface of the droplet and the solid–liquid interface advancing in diametrically opposite directions.

3. Spray deposited alloy resulted in microstructural uniformity with fine scale distribution of intermetallics in α-Al matrix. These particles have characteristic spherical morphology with variation in their size from 0.5–1 μm.

4. The structure of aluminium-rich second phase dispersoid in atomized as well as in spray deposited conditions was a cubic α-Al(Mn, Cr)Si phase. The structure and microstructure of the second phase particles was discussed in context of identification of the cubic phase as rational approximant structure of the icosahedral quasicrystal.

Acknowledgment

Support from the Department of Science and Technology sponsored project (HR/OY/P-15/97) on spray forming is gratefully acknowledged. One of the authors (AKS) would also like to thank Professor K. Chattopadhyay (IISc) and Dr. S. K. Sharma (NPL) for many useful discussions during the preparation of the manuscript.

References

1. E. J. LAVERNIA, J. D. AYERS and T. S. SRIVATSAN, *Int. Mater. Rev*. **37** (1992) 1.
2. X. LIANG, J. C. EARTHMAN and E. J. LAVERNIA, *Acta Metall. Mater*. **40** (1992) 3003.
3. S. ANNAVARAPU, D. APELIAN and A. LAWLEY, *Metall. Trans*. **19A** (1988) 3077.
4. A. K. SRIVASTAVA, in "Advances in Physical Metallurgy," edited by S. Banerjee and V. R. V. Ramanujan (Gordan and Breach Science Publ., Netherlands, 1996) p. 212.
5. A. K. SRIVASTAVA, S. N. OJHA and S. RANGANATHAN, *Metall. Mater. Trans*. **29A** (1998) 2205.
6. M. M. PARIONA, C. BOLFARINI and C. S. KIMINAMI, *Z. Metallkd*. **89** (1998) 494.
7. S. ASHOK, *Int. J. Rap. Sol*. **7** (1993) 283.
8. P. MATHUR, D. APELIAN and A. LAWLEY, *Acta Metall*. **37** (1989) 429.
9. L. D. CASTILO, Y. WU, H. M. HU and E. J. LAVERNIA, *Metall. Mater. Trans*. **30A** (1999) 1381.
10. P. S. GRANT and B. CANTOR, *Acta Metall. Mater*. **43** (1995) 913.
11. P. S. GRANT, *Prog. Mater. Sci*. **39** (1995) 497.
12. D. J. SKINNER, R. D. BYE, D. RAYBOLD and A. M. BROWN, *Scr. Metall. Mater*. **20** (1986) 867.

13. A. K. SRIVASTAVA, *J. Mater. Sci. Lett* **19** (2000) 1217.
14. S. K. DAS, in "Intermetallic Compounds, Vol. 2," edited by J. H. Westbrook and R. L. Fleischer (John Wiley & Sons, 1995) p. 175.
15. K. F. KELTON, *Int. Mater. Rev*. **38** (1993) 105.
16. M. COOPER and K. ROBINSON, *Acta Cryst*. **23** (1967) 1106.
17. K. ROBINSON, *ibid*. **5** (1952) 397.
18. L. A. DAVIS, S. K. DAS, J. C. M. LI and M. S. ZEDALIS, *Int. J. Rap. Sol*. **8** (1994) 73.
19. P. LIU, G. L. DUNLOP and L. ARNBERG, *ibid*. **3** (1987) 147.
20. T. S. LUNDY and J. F. MURDOCK, *J. Appl. Phys*. **33** (1962) 1671.
21. G. M. HOOD and R. J. SCHULTZ, *Phil. Mag*. **23** (1971) 1479.
22. P. FURRER and H. WARLIMONT, *Z. Metallkd*. **62** (1971) 100.
23. P. LIU, G. L. DUNLOP and L. ARNBERG, *Int. J. Rap. Sol*. **5** (1990) 229.
24. P. LIU and G. L. DUNLOP, *Mater. Sci. Eng*. **134A** (1991) 1182.
25. A. SINGH, A. K. SRIVASTAVA and S. RANGANATHAN, in "Microstructure of Materials," edited by K. M. Krishnan (San Francisco Press, CA, 1993) p. 152.
26. A. K. SRIVASTAVA and S. RANGANATHAN, *Acta Mater*. **44** (1996) 2935.
27. *Idem*., *Prog. Crystal Growh Charact*. **34** (1997) 251.
28. G. WATERLOO, S. J. ANDERSON and R. HOIER, IUMRS International Conference on Advanced Materials, Japan, 1993.
29. T. OHNISHI, Y. NAKATANI and K. SHINZU, *J. Jap. Inst. L. Metals* (1972) 504.
30. Y. X. GUO, R. HOIER, S. ANDERSON and O. LOHNE, *Mater. Sci. Eng*. **134A** (1991) 1215.
31. Y. X. GUO, S. J. ANDERSON, H. K. NYLUND and R. HOIER, *Micron. Microscopica Acta* **23** (1992) 165.
32. S. J. ANDERSON, Y. X. GUO, H. K. NYLUND and R. HOIER, *Electron Micros*. **2** (1992) 219.
33. O. P. PANDEY and S. N. OJHA, *Powder Metall. Int*. **23** (1991) 291.

Received 15 November 2000
and accepted 12 February 2001